Charge-induced nematicity in FeSe

Pierre Massat[a], Donato Farina[a], Indranil Paul[a], Sandra Karlsson[b,c], Pierre Strobel[b,c], Pierre Toulemonde[b,c], Marie-Aude Méasson[a], Maximilien Cazayous[a], Alain Sacuto[a], Shigeru Kasahara[d], Takasada Shibauchi[e], Yuji Matsuda[d], and Yann Gallais[a,1]

[a]Laboratoire Matériaux et Phénomènes Quantiques, CNRS UMR7162, Université Paris Diderot, Paris Cedex 13, France; [b]Institut Néél, CNRS Unité Propre de Recherche 2940, 38042 Grenoble, France; [c]Institut Néél, Université Grenoble Alpes, 38042 Grenoble, France; [d]Department of Physics, Kyoto University, Kyoto 606-8502, Japan; and [e]Department of Advanced Materials Science, University of Tokyo, Kashiwa, Chiba 277-8561, Japan

Edited by Zachary Fisk, University of California, Irvine, CA, and approved June 27, 2016 (received for review April 28, 2016)

The spontaneous appearance of nematicity, a state of matter that breaks rotation but not translation symmetry, is one of the most intriguing properties of the iron-based superconductors (Fe SC), and has relevance for the cuprates as well. Establishing the critical electronic modes behind nematicity remains a challenge, however, because their associated susceptibilities are not easily accessible by conventional probes. Here, using FeSe as a model system, and symmetry-resolved electronic Raman scattering as a probe, we unravel the presence of critical charge nematic fluctuations near the structural/nematic transition temperature, $T_S \sim 90$ K. The diverging behavior of the associated nematic susceptibility foretells the presence of a Pomeranchuk instability of the Fermi surface with d-wave symmetry. The excellent scaling between the observed nematic susceptibility and elastic modulus data demonstrates that the structural distortion is driven by this d-wave Pomeranchuk transition. Our results make a strong case for charge-induced nematicity in FeSe.

nematicity | superconductivity | Raman scattering

Electronic nematicity, whereby electrons break rotational symmetry spontaneously, is a ubiquitous property of the iron-based superconductors (Fe SC) (1). As it is often accompanied by magnetic order, an established route to nematicity is via critical magnetic fluctuations (2). However, this mechanism has been questioned in the iron–chalcogenide FeSe, where the nematic transition occurs without magnetic order, indicating a different paradigm for nematicity (3–6).

Despite its simple crystallographic structure, FeSe displays remarkable properties. Its superconducting transition temperature T_c is relatively low at ambient pressure ($\sim$ 9 K), but it reaches up to 37 K upon application of hydrostatic pressure (7, 8). Its Fermi energy is small (9–12), and in the normal state it shows bad metal behavior (9, 13). Its nematic properties are peculiar as well. The lattice distortion, elastic softening, and elastoresistvity measurements associated with the structural transition at $T_S \sim 90$ K are comparable with other Fe SC (3, 6, 11), yet NMR and inelastic neutron scattering measurements do not detect sizable low energy spin fluctuations above T_S (4, 6, 14), putting into question the spin nematic scenario envisaged in other Fe SCs (2). Although it has been argued that the magnetic scenario may still apply (15–19), there is growing interest in alternative scenario where charge or orbital degrees of freedom play a more predominant role than spins (5, 11, 20, 21). However, until now direct experimental observation of critical fluctuations associated with electronic charge or orbital nematicity in the tetragonal phase was lacking.

Here, we investigate the nature of nematicity in FeSe by using the unique ability of electronic Raman scattering to selectively probe the dynamics of electronic nematic degrees of freedom without lattice effects (22–27). We unravel the presence of critical charge nematic fluctuations in the tetragonal phase that signals the presence of a d-wave Pomeranchuk instability of the Fermi surface (28). The extracted nematic susceptibility shows quantitative scaling with the measured lattice softening (6, 29), demonstrating that charge nematic fluctuations account entirely for the lattice instability. Our results make a strong case for itinerant electronic charge driven nematicity in FeSe.

Raman scattering is a photon-in photon-out process, whereby a monochromatic visible light is inelastically scattered at a different frequency by dynamical fluctuations of the electrical polarizability of the sample (Fig. 1*A*). In metals the Raman spectra at low frequency shifts are typically composed of sharp optical phonon peaks superimposed on a broad electronic background, generally referred to as electronic Raman scattering (ERS). The ERS intensity measures the long wavelength dynamical charge correlation function in the symmetry channel μ: $S_\mu(\omega) \equiv \langle \rho_\mu^\dagger(\omega)\rho_\mu(\omega)\rangle$, where ω is the frequency (or Raman) shift between incoming and scattered photons, ρ_μ is the form-factor–weighted electronic charge (30), and † is the Hermitian conjugate. The fluctuation–dissipation theorem in turn links the measured correlation function S_μ to the imaginary part of the Raman response function χ''_μ: $S_\mu(\omega) = \frac{1}{\pi}[1 + n_B(\omega, T)]\chi''_\mu(\omega)$, where n_B is the Bose function.

Because it is a symmetry-resolved probe of the charge fluctuation dynamics with zero momentum transfer, electronic Raman scattering is ideally suited to detect critical in-plane charge nematic fluctuations (22, 23). The symmetry of the charge fluctuations μ probed in a Raman experiment is fixed by the directions of the incoming and scattered photon polarizations. Of interest here is the B_{1g} symmetry (using 1 Fe/cell notation; Fig. 1*B*), obtained for photons polarized along the diagonals of the Fe–Fe bonds and which transforms as $k_x^2 - k_y^2$. The B_{1g} charge nematic fluctuations probed by Raman are equivalent to a Fermi surface deformation with d-wave symmetry. This electronic instability was predicted by Pomeranchuk to occur in an isotropic Fermi liquid in which the Fermi surface spontaneously deforms

Significance

Anisotropic electron liquids are ubiquitous in many correlated electron systems. Among them, electron nematics, which break rotation but not translation symmetry, are believed to play a key role in the physics of both cuprates and iron-based superconductors (Fe SC). However the study of electron nematicity has been hampered by the lack of an adequate probe of its associated fluctuations and susceptibility, making it difficult to track its origin. Here, using polarization-resolved Raman scattering, we report the detection of critical nematic fluctuations in the charge channel in the Fe SC compound FeSe. The strong enhancement of the associated nematic susceptibility allows us to link the appearance of nematicity to a symmetry-breaking distortion of the Fermi surface.

Author contributions: Y.G. designed research; P.M., D.F., I.P., S. Karlsson, P.S., P.T., S. Kasahara, T.S., Y.M., and Y.G. performed research; P.M., I.P., M.-A.M., M.C., A.S., and Y.G. analyzed data; and I.P. and Y.G. wrote the paper.

The authors declare no conflict of interest.

This article is a PNAS Direct Submission.

[1]To whom correspondence should be addressed. Email: yann.gallais@univ-paris-diderot.fr.

This article contains supporting information online at www.pnas.org/lookup/suppl/doi:10.1073/pnas.1606562113/-/DCSupplemental.

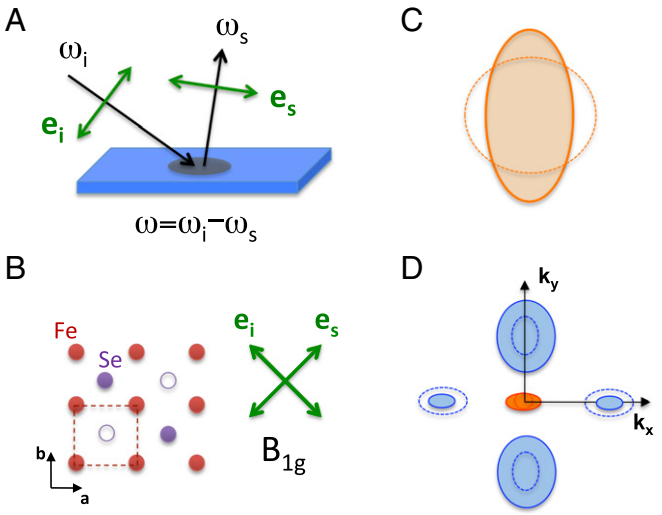

Fig. 1. (*A*) Schematic of the Raman scattering process with incoming and scattered photons of frequency $\omega_{i/s}$ and polarization $\mathbf{e}_{i/s}$, respectively. The Raman shift is defined as the frequency shift between the incoming and scattered photon frequencies. (*B*) FeSe *ab* plane with Se atoms alternating above and below the plane defined by the Fe atoms. The 1 Fe unit cell, which neglects the alternating Se atoms, is drawn in dotted lines. In the tetragonal phase above T_S, $a = b$, and the crystal structure of FeSe has a fourfold symmetry axis. The B_{1g} symmetry is obtained using crossed incoming and scattered photon polarizations at 45 degrees of the Fe–Fe bonds. (*C*, *D*) Fermi surface deformation associated to a d-wave Pomeranchuk order for (*C*) an isotropic Fermi liquid and (*D*) the multiband Fe SC showing d-wave-like deformations with global B_{1g} symmetry which break the fourfold symmetry axis. The deformations shown are consistent with ARPES measurements in the orthorhombic phase of FeSe (32): and the hole pocket (red) expand along one direction, the elliptical electron pockets (blue) shrink (expand) along the same (other) direction. The 1 Fe unit cell is used.

along a specific direction, breaking rotational symmetry (28) (Fig. 1*C*). In the context of Fe SC, the B_{1g} Raman response probes the fluctuations associated to a multiband version of a d-wave Pomeranchuk-order parameter that breaks the fourfold symmetry axis (Fig. 1*D*): $\rho_{B_{1g}} = \sum_{k,\alpha} f_k n_{k,\alpha}$ where α is the orbital index, f_k a d-wave form factor that transforms as $k_x^2 - k_y^2$, and n_k the electron density (25).

Raman scattering experiments were performed on two different FeSe crystals (SP208 and MK; *Supporting Information* and refs. 31 and 32). Fig. 2*A* displays the Raman response χ''_μ in different symmetries μ as a function of temperature in the tetragonal phase ($T > T_S$) for SP208. For comparison besides the response in B_{1g} symmetry, we also show the response in B_{2g} and A_{1g} symmetries which transform as $k_x k_y$ and $k_x^2 + k_y^2$ respectively (see form factors in Fig. 2*A*, *Inset*). Upon cooling the $\mu = B_{1g}$ Raman response displays an overall enhancement over a wide energy range extending up to 2,000 cm^{-1}. At high temperature the response is dominated by a broad peak, centered around 400 cm^{-1} and the weight of which increases on cooling. In addition, a relatively sharp peak emerges below 100 cm^{-1}: it softens and gains considerably in intensity upon approaching T_S (Fig. 2*B*). By contrast, the response in the two other configurations is only mildly temperature dependent. The B_{2g} response shows a weak suppression above 500 cm^{-1} and a build up of spectral weight between 200 and 250 cm^{-1}, which likely originates from an interband transition between nearly parallel spin-orbit split hole bands at the Γ point (11, 33). Below T_S the B_{1g} response strongly reconstructs (Fig. 2*C*): the low energy response is suppressed and there is a weak transfer of spectral weight at higher energy, above 500 cm^{-1}, in agreement with a previous Raman study (34). Below T_c superconducting gaps open on the different Fermi pockets (Fig. 2*C*, *Inset*) giving rise to two sharp peaks at $2\Delta = 28\ (\pm 1)$ cm^{-1} (~ 3.5 meV) and 37 (± 2) cm^{-1} (~ 4.6 meV), in broad agreement with scanning tunneling microscopy measurements (9).

Focusing on the tetragonal phase, we use the fact that the Raman responses at finite frequency can be translated into their corresponding symmetry-resolved charge susceptibilities at zero frequency using the Kramers–Kronig relation:

$$\chi_\mu(T) = \frac{2}{\pi}\int_0^\Lambda \frac{\chi''_\mu(T,\omega)}{\omega} d\omega. \qquad [1]$$

The susceptibilities obtained by integrating the finite frequency responses up to $\Lambda = 2{,}000$ cm^{-1} are shown as a function of temperature in Fig. 3. Although the B_{2g} and A_{1g} susceptibilities are nearly T independent, the B_{1g} susceptibility $\chi_{B_{1g}}$ shows a strong enhancement with lowering temperature and subsequently collapses below T_S. This demonstrates the growth of charge nematic fluctuations in the tetragonal phase, which are arrested by the structural transition at T_S. For both SP208 and MK crystals the temperature dependence of $\chi_{B_{1g}}$ above T_S is well captured by a Curie–Weiss law $\chi_{B_{1g}}(T) = \frac{B}{T - T_0}$, with a Curie–Weiss temperature T_0 significantly below T_S, namely 8 and 20 K for SP208 and MK, respectively.

A key step in the data interpretation is that the nematic fluctuations described above are entirely electronic in origin, and are not affected by the fluctuations of the orthorhombic strain $u_{xx} - u_{yy}$, where $\hat{u}$ is the lattice strain tensor (25). The lattice fluctuations are coupled to the electronic Pomeranchuk order parameter $\rho_{B_{1g}}$ via the electron–phonon interaction $\mathcal{H}_{\text{el-ph}} = \lambda \rho_{B_{1g}}(u_{xx} - u_{yy})$, where λ is the coupling constant. The full, measured nematic susceptibility at momentum $\mathbf{q}$ along the relevant high-symmetry direction and frequency ω can be expressed as

$$\left(\chi_{B_{1g}}\right)^{-1}(\mathbf{q},\omega) = \left(\chi^0_{B_{1g}}\right)^{-1}(\mathbf{q},\omega) - \frac{\lambda^2 q^2}{C_S^0 q^2 - \omega^2}. \qquad [2]$$

Here $\chi^0_{B_{1g}}(\mathbf{q},\omega)$ is the electronic susceptibility associated with $\rho_{B_{1g}}$ in the absence of the lattice, and the second term is the contribution of the orthorhombic strain with the elastic shear modulus C_S^0. Crucially, the nematic susceptibility obtained from the finite frequency Raman spectra ($\omega > 8$ cm^{-1}) using Eq. **1** is in the dynamical limit, i.e., $\chi_\mu(T) = \lim_{\omega\to 0}\chi_\mu(T,\omega,q=0)$. In this limit the second term of Eq. **2** vanishes, implying that the extracted nematic susceptibility does not couple to the orthorhombic strain fluctuations (24, 25, 35) and, therefore, T_0 represents the bare electronic charge nematic transition temperature that is unrenormalized by the lattice. We conclude that the observed Curie–Weiss behavior demonstrates the presence of a d-wave Pomeranchuk instability of purely electronic origin in FeSe. This is in agreement with a recent renormalization group analysis, which shows that the leading instability is in the Pomeranchuk channel in low Fermi energy systems like FeSe (36). The d-wave Pomeranchuk order may explain the peculiar k-dependent orbital splitting observed by angle-resolved photoemission spectroscopy (ARPES) below T_S, which does not fit a simple ferro-orbital order (11, 32, 33).

Having established the presence of critical charge nematic fluctuations, we proceed to show that the structural instability at T_S is entirely driven by the reported charge nematic softening. The renormalization of the relevant shear modulus C_S due to the above-mentioned symmetry-allowed electron–lattice coupling is given by (6, 25)

$$C_S(T) = C_S^0 - \lambda^2 \chi_{B_{1g}}(T), \qquad [3]$$

where $\chi_{B_{1g}}$ is the measured charge nematic susceptibility as defined in Eq. **1**. We take C_S^0, the bare modulus, to be T -independent as expected for a purely electronic-driven structural transition thus

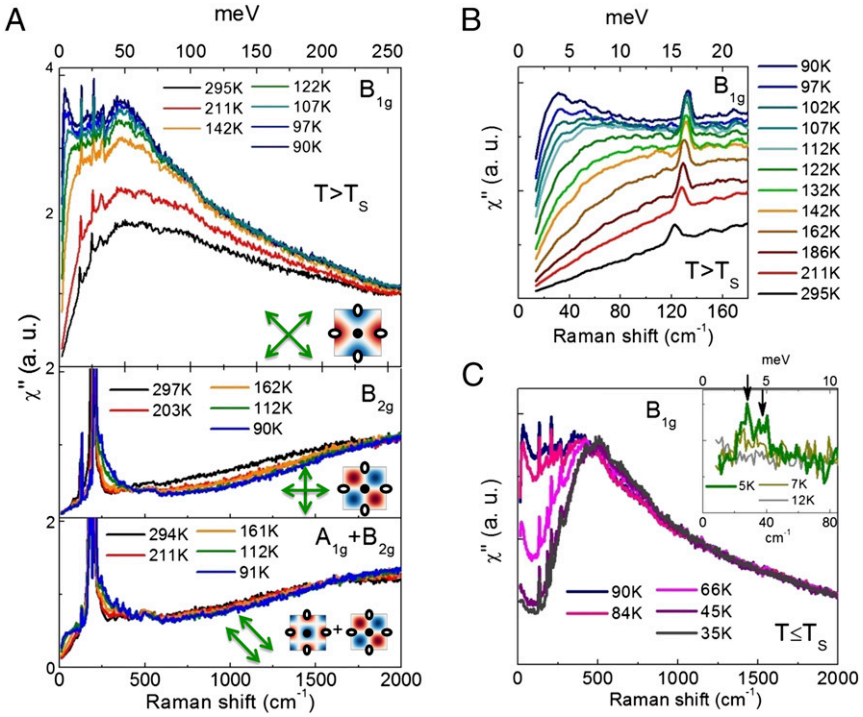

Fig. 2. (*A*) Symmetry-dependent Raman spectra of FeSe (SP208 crystal) above T_S = 87 K using 2.33 eV photons. The sharp peaks superimposed on the electronic continuum are due to Raman active optical phonons. Also shown in *Inset* are the schematics k-space structures of the Raman form factors in different symmetries (blue and red colors indicate positive and negative amplitudes, respectively), and the polarization configurations used to select them. (*B*) Temperature dependence of the low energy B_{1g} spectra above T_S. (*C*) Evolution of the B_{1g} spectra across T_S. The *Inset* shows the spectra across the superconducting transition at T_c = 8.5 K (SP208). The arrows indicate 2Δ superconducting peaks.

leaving λ as the only free parameter. As shown in Fig. 4, we find an excellent agreement between the observed softening of C_S, obtained either directly from ultrasound measurements (29), or indirectly from Young's modulus measurements (6), and $\chi_{B_{1g}}(T)$ obtained from our Raman measurements. Together with the absence of scaling between elastic modulus and spin fluctuations, our result makes a strong case for a lattice distortion in FeSe induced by a d-wave Pomeranchuk instability of the Fermi surface.

Next, we discuss the frequency dependence of the B_{1g} response in the tetragonal phase. As is evident from the spectra close to T_S in Fig. 2*A*, the B_{1g} response is composed of two contributions, a sharp quasi-elastic peak (QEP) at low energy (below 200 cm^{-1}), and a much broader peak centered around 400 cm^{-1}. Both features appear only in the B_{1g} symmetry: $\chi''_{B_{1g}}(\omega) = \chi''_{QEP}(\omega) + \chi''_b(\omega)$. The

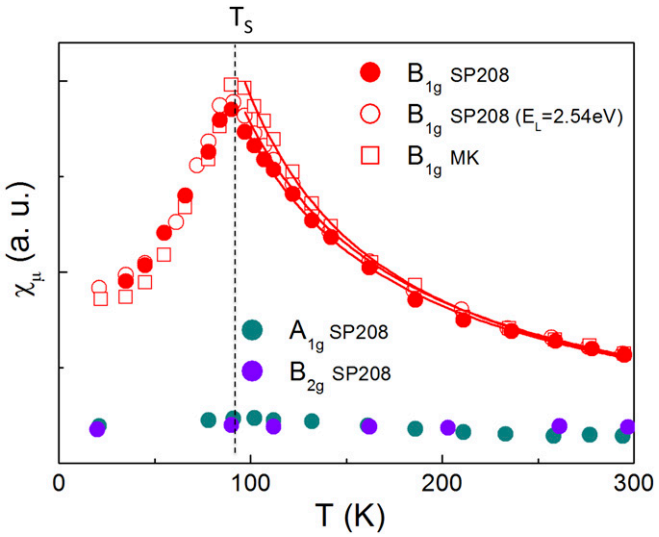

Fig. 3. Temperature dependence of the B_{1g} charge nematic susceptibility for SP208 (T_S = 87 K) and MK (T_S = 88.5 K) using 2.33 eV photons. Also shown are data on SP208 using a different excitation energy (2.54 eV) and the susceptibility in the other symmetry channels on SP208 (A_{1g} and B_{2g}). The lines are Curie–Weiss fits of the B_{1g} susceptibility above T_S.

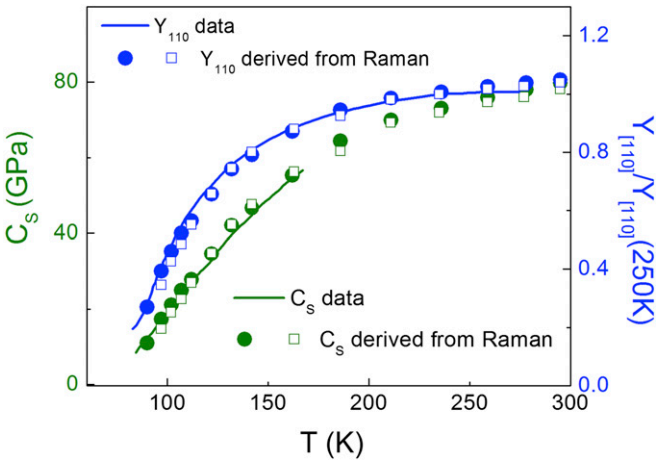

Fig. 4. Shear modulus C_S (29) and Young's modulus $Y_{[110]}$ (6) data (line) and corresponding simultaneous fits using the nematic susceptibility $\chi_{B_{1g}}$ extracted from Raman scattering using Eqs. **1** and **3**. Full/open symbols correspond to Raman data on SP208/MK crystal. The λ values (in relative units) used for the two crystals agree within 10%. The standard relationship between $Y_{[110]}$ and C_S was used (6) (see *Supporting Information* for details).

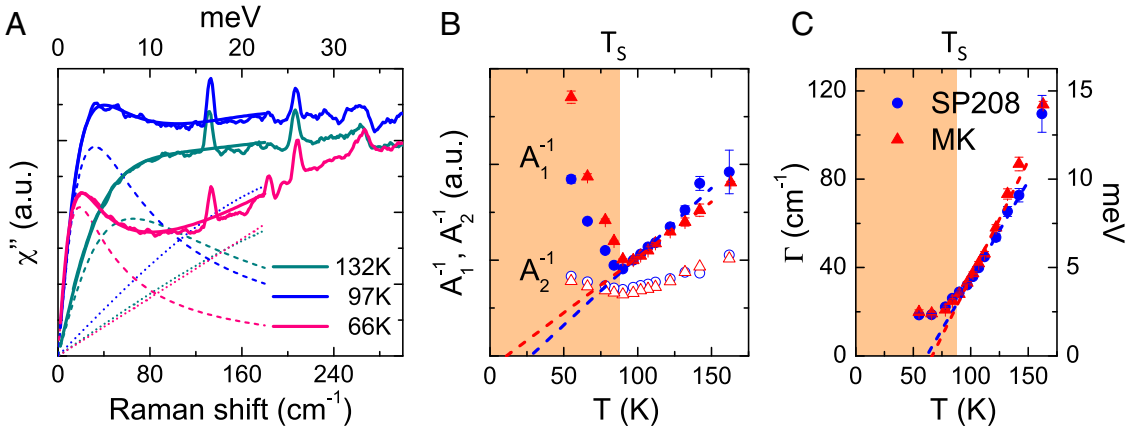

Fig. 5. (*A*) Low energy fits of the B_{1g} response of SP208 using a damped Lorentzian for the QEP and an odd in frequency third-order polynomial for the low energy part of the broad peak (*Supporting Information*). (*B*) Temperature dependence of the inverse of the two contributions to the nematic susceptibility, A_1^{-1} and A_2^{-1} for SP208 (blue dots) and MK (red triangle). The dashed line is a linear fit of A_1^{-1} between T_S and 150 K. (*C*) Temperature dependence of the QEP line width Γ_1. The dashed line is a linear fit between T_S and 150 K.

low energy QEP is well reproduced by a damped Lorentzian $\chi''_{QEP}(\omega) = A_1 \frac{\omega\Gamma}{\omega^2+\Gamma^2}$, which allows a clear separation of the two contributions, and the extraction of the broad $\chi''_b(\omega)$ close to T_S (Fig. 5*A*, *Supporting Information*). As shown in Fig. 5*B*, their respective contributions $A_1(T)$ and $A_2(T)$ to the nematic susceptibility $\chi_{B_{1g}}(T)$, through Eq. **1**, have different behavior close to T_S in the tetragonal phase. Only the QEP contribution is critical, with $A_1(T)^{-1}$ extrapolating to zero close to T_0. In contrast, the broad peak contribution $A_2(T)$, although sizable, increases only mildly upon cooling. In addition, the extracted QEP line width $\Gamma(T)$ shows a strong softening and extrapolates to zero at ~65 K (Fig. 5*C*).

In a weak coupling description of a d-wave Pomeranchuk instability, the QEP can be understood as the standard Drude contribution to the Raman conductivity $\chi''_{B_{1g}}(\omega)/\omega$ with weight A_1 and width Γ that are renormalized by the diverging nematic correlation length ξ (25). Defining $r_0 \equiv \xi^{-2} \propto (T - T_0)$, this theory predicts $A_1^{-1} \propto r_0$, and $\Gamma \propto \Gamma_0 r_0$, where Γ_0 is a single particle scattering rate. As shown in Fig. 5 *B* and *C*, the linear temperature dependencies of A_1^{-1} and Γ between T_S and T_S + 60 K are in agreement with the above expectation. However, the two quantities extrapolate to zero at different temperatures 20 K (± 10 K) and at 65 K (± 5 K) respectively. We attribute this mismatch to a strong linear temperature dependence of the scattering rate $\Gamma_0(T)$, as suggested by resistivity measurements (9, 31) (*Supporting Information*).

Finally we discuss the microscopic origin of the broad feature. It is unlikely to be from an Azlamazov–Larkin-type contribution of the fluctuations of the stripe magnetic state (24, 27, 37, 38) because, below T_S, inelastic neutron scattering and NMR data suggest an enhancement of low energy spin fluctuations (4, 6, 14), whereas we observe a shift of spectral weight of $\chi''_b(\omega)$ to higher frequencies. It is also unlikely that the feature is an interband transition, because $\chi''_b(\omega)$ does not show any gap at low frequencies above T_S (*Supporting Information*). One possibility is that it is the nematic response of electrons that are not sharply defined quasiparticles. Such an interpretation would be in line with the observed bad metal behavior (9, 13), and the fact that the Fermi energy of FeSe is rather small (9, 11, 12).

Overall, our findings support a scenario in which the nematic transition of FeSe is due to an incipient d-wave Pomeranchuk instability of the Fermi surface. This provides an alternative route to nematicity compared with the prevailing spin fluctuation–mediated scenario that has been proposed for other Fe SC. The subsequent challenge will be to identify the microscopic interaction that is responsible for the Pomeranchuk instability, and to study if such an interaction is relevant for other Fe SC as well.

Materials and Methods

Single crystals of FeSe were grown using the chemical vapor transport method based on the use of an eutectic mixture of $AlCl_3$/KCl as described in refs. 9, 31. The two different single crystals measured were grown in Grenoble (SP208) and Kyoto (MK). Polarization-resolved Raman experiments have been carried out using a diode-pumped solid state (DPSS) laser emitting at 2.33 eV. For low energy (< 500 cm^{-1}) measurements, a triple-grating spectrometer equipped with 1,800 grooves/mm gratings and a nitrogen-cooled CCD camera were used. Measurements at higher energies, up to 2,000 cm^{-1}, were performed using a single-grating spectrometer with 600 grooves/mm in combination with an ultrasteep edge filter (Semrock) to block the stray light. Additional measurements were also performed using the 2.54 eV line of an Ar-Kr Laser.

ACKNOWLEDGMENTS. We thank G. Blumberg, V. Brouet, A. V. Chubukov, V. D. Fil, R. Hackl, and J. Schmalian for fruitful discussions. P.M., M.-A.M., M.C., A.S., and Y.G. acknowledge financial support from ANR Grant "Pnictides," from a Labex SEAM grant, and from a SESAME grant from région Ile-de-France. P.T. and S. Karlsson acknowledge the financial support of UJF (now integrated inside "Université Grenoble Alpes") and Grenoble INP (through the AGIR-2013 contract of S. Karlsson). S. Kasahara., T.S., and Y.M. acknowledge the support of Grants-in-Aid for Scientific Research (KAKENHI) from Japan Society for the Promotion of Science (JSPS), and the Topological Quantum Phenomena (25103713) Grant-in-Aid for Scientific Research on Innovative Areas from the Ministry of Education, Culture, Sports, Science and Technology (MEXT) of Japan.

1. Chu J-H, et al. (2010) In-plane resistivity anisotropy in an underdoped iron arsenide superconductor. *Science* 329(5993):824–826.
2. Fernandes RM, Chubukov AV, Schmalian J (2014) What drives nematic order in iron-based superconductors? *Nat Phys* 10:97–104.
3. McQueen TM, et al. (2009) Tetragonal-to-orthorhombic structural phase transition at 90 K in the superconductor Fe(1.01)$Se_{.1.01}$. *Phys Rev Lett* 103(5):057002.
4. Imai T, Ahilan K, Ning FL, McQueen TM, Cava RJ (2009) Why does undoped FeSe become a high-Tc superconductor under pressure? *Phys Rev Lett* 102(17):177005.
5. Baek S-H, et al. (2015) Orbital-driven nematicity in FeSe. *Nat Mater* 14(2):210–214.
6. Böhmer AE, et al. (2015) Origin of the tetragonal-to-orthorhombic phase transition in FeSe: A combined thermodynamic and NMR study of nematicity. *Phys Rev Lett* 114(2): 027001.
7. Medvedev S, et al. (2009) Electronic and magnetic phase diagram of β-Fe(1.01)Se with superconductivity at 36.7 K under pressure.$_{1.01}$. *Nat Mater* 8(8):630–633.
8. Garbarino G, et al. (2009) High-temperature superconductivity (Tc onset at 34 K) in the high-pressure orthorhombic phase of FeSe. *EPL* 86:27001.
9. Kasahara S, et al. (2014) Field-induced superconducting phase of FeSe in the BCS-BEC cross-over. *Proc Natl Acad Sci USA* 111(46):16309–16313.
10. Terashima T, et al. (2014) Anomalous Fermi surface in FeSe seen by Shubnikov-de Haas oscillation measurements. *Phys Rev B* 90:144517.
11. Watson MD, et al. (2015) Emergence of the nematic electronic state in FeSe. *Phys Rev B* 91:155106.
12. Audouard A, et al. (2015) Quantum oscillations and upper critical magnetic field of the iron-based superconductor FeSe. *EPL* 109:27003.

13. Aichhorn M, Biermann S, Miyake T, Georges A, Imada M (2010) Theoretical evidence for strong correlations and incoherent metallic state in FeSe. *Phys Rev B* 82:064504.
14. Wang Q, et al. (2016) Strong interplay between stripe spin fluctuations, nematicity and superconductivity in FeSe. *Nat Mater* 15(2):159–163.
15. Glasbrenner JK, et al. (2015) Effect of magnetic frustration on nematicity and superconductivity in iron chalcogenides. *Nat Phys* 11:953–957.
16. Wang F, Kivelson S, Lee D-H (2015) Nematicity and quantum paramagnetism in FeSe. *Nat Phys* 11:959–963.
17. Chubukov AV, Fernandes RM, Schmalian J (2015) Origin of nematic order in FeSe. *Phys Rev B* 91:201105.
18. Yu R, Si Q (2015) Antiferroquadrupolar and Ising-nematic orders of a frustrated bilinear-biquadratic Heisenberg model and implications for the magnetism of FeSe. *Phys Rev Lett* 115(11):116401.
19. Yamakawa Y, Omari S, Kontani H (2016) Nematicity and magnetism in FeSe and other families of Fe-based superconductors. *Phys Rev X* 6:021032.
20. Jiang K, Hu J-P, Ding H, Wang Z (2016) Interatomic Coulomb interaction and electron nematic bond order in FeSe. *Phys Rev B* 93:115138.
21. Su Y, Liao H, Li T (2015) The form and origin of orbital ordering in the electronic nematic phase of iron-based superconductors. *J Phys Condens Matter* 27(10):105702.
22. Yamase H, Zeyher R (2013) Electronic Raman scattering from orbital nematic fluctuations. *Phys Rev B* 88:125120.
23. Gallais Y, et al. (2013) Observation of incipient charge nematicity in Ba(Fe(1-x)Co(x))2As2. *Phys Rev Lett* 111(26):267001.
24. Kontani H, Yamakawa Y (2014) Linear response theory for shear modulus C66 and Raman quadrupole susceptibility: Evidence for nematic orbital fluctuations in Fe-based superconductors. *Phys Rev Lett* 113(4):047001.
25. Gallais Y, Paul I (2016) Charge nematicity and electronic Raman scattering in iron-based superconductors. *C R Phys* 17:113–139.
26. Thorsmølle VK, et al. (2016) Critical charge fluctuations in iron pnictide superconductors. *Phys Rev B* 93:054515.
27. Kretzschmar F, et al. (2016) Critical spin fluctuations and the origin of nematic order in Ba(Fe1-xCox)2As2. *Nat Phys* 12:560–563.
28. Pomeranchuk IJ (1958) On the stability of a Fermi liquid. *Sov Phys JETP* 8:361.
29. Zvyagina GA, et al. (2013) Acoustic characteristics of FeSe single crystals. *EPL* 101:56005.
30. Devereaux TP, Hackl R (2007) Inelastic light scattering from correlated electrons. *Rev Mod Phys* 79:175.
31. Karlsson S, et al. (2015) Study of high-quality superconducting FeSe single crystals: Crossover in electronic transport from a metallic to an activated regime above 350 K. *Supercond Sci Technol* 28:105009.
32. Suzuki Y, et al. (2015) Momentum-dependent sign-inversion of orbital polarization in superconducting FeSe. *Phys Rev B* 92:205117.
33. Zhang P, et al. (2015) Observation of two distinct dxz=dyz band splittings in FeSe. *Phys Rev B* 91:214503.
34. Gnezdilov V, et al. (2013) Interplay between lattice and spin states degree of freedom in the FeSe superconductor: Dynamic spin state instabilities. *Phys Rev B* 87:144508.
35. Gallais Y, Paul I, Chauvière L, Schmalian J (2016) Nematic resonance in the Raman spectrum of iron-based superconductors. *Phys Rev Lett* 116(1):017001.
36. Chubukov AV, Khodas M, Fernandes RM (2016) Magnetism, superconductivity, and spontaneous orbital order in iron-based superconductors: Who comes first and why? arXiv:1602.05503.
37. Khodas M, Levchenko A (2015) Raman scattering as a probe of nematic correlations. *Phys Rev B* 91:235119.
38. Karahasanovic U, et al. (2015) Manifestation of nematic degrees of freedom in the Raman response function of iron pnictides. *Phys Rev B* 92:075134.
39. Maksimov AA, et al. (1992) Investigations of the temperature dependence of the low energy electronic Raman scattering in Ti2Ba2CaCu2O8 single crystals. *Solid State Commun* 81:407.
40. Yoshizawa M, et al. (2012) Structural quantum criticality and superconductivity in iron-based superconductor Ba(Fe1 xCox)2As2. *J Phys Soc Jpn* 81:024604.
41. Simayi S, et al. (2013) Strange inter-layer properties of Ba(Fe1-xCox)2As2 appearing in ultrasonic measurements. arXiv:1310.2681.
42. Chandra S, Islam AKMA (2010) Elastic properties of mono- and poly-crystalline PbO-type FeSe1-xTex (x = 0-1.0): A first-principles study. *Physica C* 470:2072.